JOURNAL OF AIRCRAFT
Vol. 42, No. 1, January–February 2005

Global Model Approach for X-31 VECTOR System Identification

Detlef Rohlf*
DLR, German Aerospace Research Center, 38108 Brunswick, Germany

A global model approach developed on data from the experimental aircraft program X-31 EFM was recently improved during the X-31 VECTOR program. Both programs are briefly presented, focusing on extremely precise ESTOL landings following a slow, thrust-vectored approach at high angle of attack. High-accuracy navigation and inertial sensor systems enable onboard calculation of the height above runway with sufficient accuracy, which is also required to identify ground effect. System identification procedure utilizes a global model to cover the entire flight regime including high-lift configuration during power approach and landing. Analysis of specially designed flight tests led to aerodynamic increment tables for supplementary update of the original database. The wind-tunnel and computational fluid dynamics (CFD) predicted ground effect was incorporated into the highly accurate identified global model, which was then used for conventional landings resimulation to support the initial extremely short takeoff and landing (ESTOL) to the ground flight clearance process. Recently an incremental ground effect model was implemented to supplement the original data set. First identification results from conventional and ESTOL landings show some improvements compared to the predictions at very low height above ground.

Introduction

DURING envelope expansion flight tests, simulation models are to be verified and, if necessary, updated based on the flight-test results. System identification has proved to be an effective tool for this task, but in general, it is restricted to flight tests with relatively small deviations around the tested reference conditions, and the database update is performed in a separated step. To overcome these restraints, a global model identification concept was developed that uses the original database and enables incremental updates where necessary. The entire flight regime including takeoff and landing is covered allowing a step-by-step or a single-step modification depending on flight-test progress. This necessitates integration of generic subsystem models, for example, engine and landing gear dynamics. In this paper, the general idea of global model is presented, highlighting selected results without going into all of the details.

Background

During the X-31 enhanced fighter maneuverability (EFM) program, an experimental aircraft of the famous X-series has been realized with international partnership.[1] Two X-31A aircraft, built by The Boeing Company (formerly Rockwell International) and EADS (formerly MBB),[2] have demonstrated the concept of EFM, impressively (Fig. 1) in more than 550 flights since their maiden flights in Southern California in 1990.[3] Final highlight of that program was the participation at the 1995 Paris Le Bourget Airshow.

After the EFM project, the X-31A aircraft was mothballed and reactivated for the Vectoring ESTOL Control Tailless Operation Research Program (VECTOR) to demonstrate ESTOL and to test a novel flush air data system (FADS).[4,5] Several modifications were necessary to accomplish these tasks, including a flight control software redesign with autothrottle integration and installation of a new inertial navigation system augmented by a high-precision differential global positioning system (DGPS). External changes are the noseboom relocation, nose cone reshaping to house FADS, and a new painting (Fig. 2). The X-31 VECTOR version was first flown on 17 May 2002 and has performed 73 sorties culminating in the fully automated 24-deg ESTOL landing on 29 April 2003, at Patuxent River Naval Air Station, Maryland.

The X-31A is an aerodynamically unstable delta-wing/canard configuration with extremely high maneuverability and outstanding flying qualities. Using a thrust vectoring (TV) system[6] and an innovative flight control design,[7] X-31A aircraft can be flown within the so-called poststall regime (PST), that is, well beyond the conventional stall barrier up to 70-deg angle of attack. Although the aerodynamic control devices lack efficiency in this low-speed range, the aircraft is fully controllable and maneuverable through the TV system, which deflects the engine exhaust flow using temperature-resistant composite vanes. The installed power plant is a General Electric F404-GE-400 engine with afterburner and typical takeoff weight is approximately 7000 kg.

The DLR Institute of Flight Systems participated in both the X-31 EFM and VECTOR programs under contracts from German Ministry of Defense and Procurement (BMVg/BWB) and EADS.[8,9] Besides contributions to general flight-test data analysis,[10] it was involved in the system identification effort with special attention on the determination of aerodynamic stability and control derivatives. This task includes development of adequate model structures and estimation of associated parameters and is based on special designed flight tests. If the results of such flight tests do not validate the CFD and wind-tunnel predictions within certain tolerances, aerodynamic updates become necessary. Subsequently, these updates may require further control law adjustments and renewed stability analysis.

Identification Procedure and Global Model

As mentioned, system identification incorporates a global model covering the entire X-31A flight regime from low subsonic flight conditions with extreme high angles of attack (AOA) maximum of 70 deg up to the low super sonic flight conditions (maximum Mach number ~1.3). The complex aircraft aerodynamics comprises 1) conventional and high-AOA aerodynamics, 2) unsteady flow separations at high AOA, 3) cruise and high-lift configurations, 4) landing gear influences, 5) ground effect, and 6) drag chute aerodynamics.

To enable separation of the aerodynamic parameters throughout large-amplitude maneuvers and aircraft configuration changes, generic subsystems have been utilized to deal with 1) sensor time delays and calibrated data obtained from preceding flight path reconstruction, 2) weight and balance calculations considering the fuel slosh, 3) engine dynamics, 4) thrust vector calculations, 5) aircraft configuration transitions, 6) landing gear suspension dynamics, and 7) drag chute filling characteristics.

The global model utilizes the original database and application rules as in the simulations, for example, aerodynamics derived from

Received 24 November 2003; revision received 19 March 2004; accepted for publication 29 March 2004.

*Research Scientist, Institute of Flight Systems, Lilienthalplatz 7.

Fig. 1 X-31A at 70-deg angle of attack (EFM).

Fig. 2 X-31A during 24-deg ESTOL landing (VECTOR).

wind-tunnel tests and a table-based thrust model, which are adapted to flight data evaluation and supplemented by increments applying a regression method (Fig. 3).[11] Therefore, flight-measured aircraft states, control surface deflections, etc., are used to resimulate the flight-measured aircraft accelerations, and their deviations are minimized. A beforehand data compatibility check ensures that the measurements are consistent and error free. As well known, it is moreover indispensable to apply actual values for aircraft weight, center of gravity and moments of inertia, which change in the course of flight because of the decreasing fuel quantity. Depending on center of gravity are the lever arms of the various sensors such as accelerometers and noseboom-mounted airflow sensors. Center of gravity and moments of inertia are additionally affected by landing gear retraction and extension.

Input Signal: Generation and Characteristics

For identification of aerodynamics of an highly augmented aircraft with synchronically deflected control effectors, it is not sufficient to excite the system characteristic frequencies for determination of stability derivatives. In addition, it is indispensable to stimulate each individual control surface separately for determination of individual control derivatives.[12] Therefore, specially designed and optimized input signals are necessary, which, as in the case of X-31 VECTOR, may be generated in a supplementary part of the flight control software (Fig. 4) and which can be selected and activated

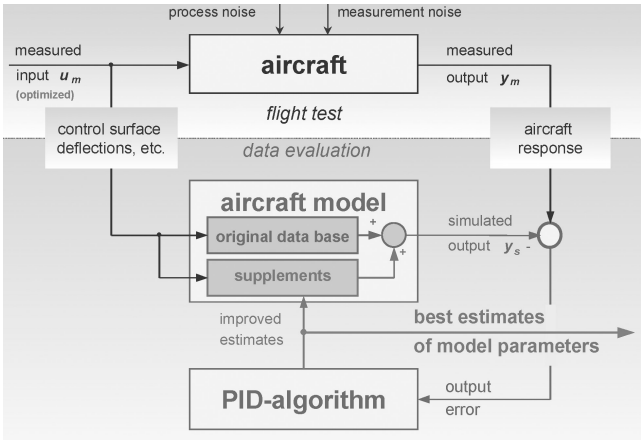

Fig. 3 Aerodynamic parameters identification procedure.

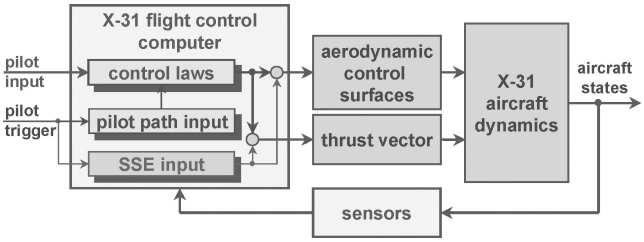

Fig. 4 Integration of system identification input sequences into the flight control system.

by the pilot during the flight test. The input in the pilot command path runs through the flight control laws just as a regular pilot control input and is distributed to the individual control surfaces, that is blended, depending on flight conditions and corresponding control surface effectiveness. The separated surface excitation (SSE), however, bypasses the flight control laws and results in uncorrelated deflections of the selected control surface.

To generate effective excitations, although not too large (i.e., to meet given maneuver limits and to avoid structural overloads), input signal amplitudes are calculated depending on measured dynamic pressure. Figure 5 shows time histories of a typical input sequence from X-31 VECTOR flight test. In the pilot path, a multistep 1123 signal is used to get relatively broad-banded excitations of the different characteristic motion frequencies. The 1123 signal is a modification of the widely used 3211 signal, designed with balanced positive and negative areas and time twisted to place the excitation with the higher frequency close to the initially adjusted reference flight conditions. For determination of the control surfaces effectiveness, a shorter 121 signal is used. This signal produces sharp-edged aircraft reactions around the reference point, which can be attributed to each individual control surface deflection. To prevent rate saturation in the electrohydraulic actuators, the slope of 121 signal is limited.

Fuel Slosh Impact

The measurement of fuel quantity and center of gravity location are significantly affected by fuel slosh due to the unique design of the X-31A fuel tank, which is built around the engine's air intake tube (Fig. 6).

Measured Fuel Quantity

Measured fuel quantity is used as input for the weight and balance calculations to deal with the weight decrease due to fuel consumption. To allow determination of a corrected fuel quantity signal, it is obligatory to model and identify the measurement errors. This calls in turn for numerical integration of the fuel flow with initial value estimation. Because the measured fuel flow does not account for after-burner fuel consumption, it is necessary to estimate the latter additionally. The required after-burner on/off signal is taken from

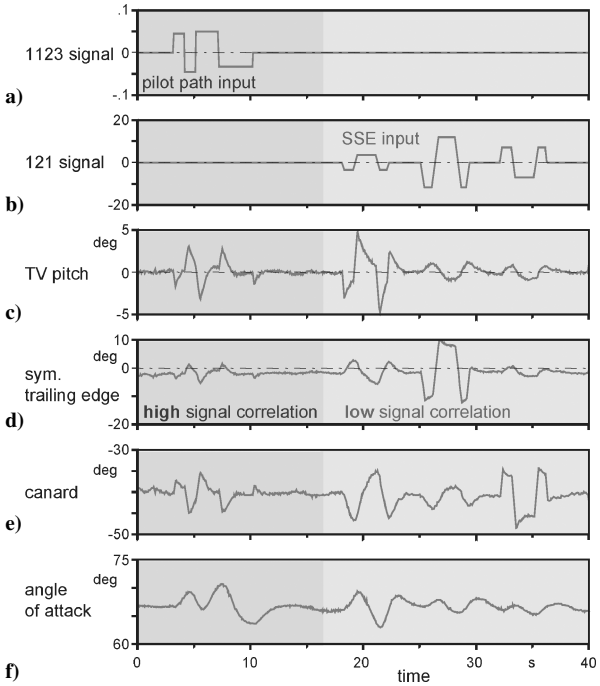

Fig. 5 Input sequence for excitation of longitudinal aircraft motion.

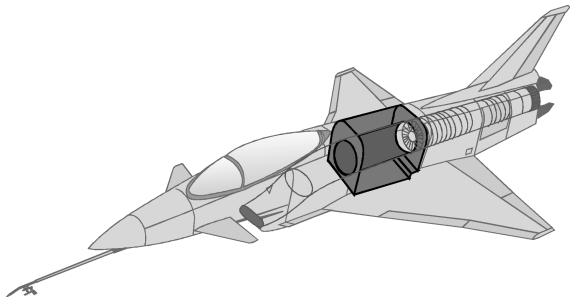

Fig. 6 X-31A fuel tank installation.

the respective output of the dynamic engine model, described in the following section.

Figure 7 shows the fuel slosh impact on the measured fuel quantity and the determined true fuel quantity signal. Seven time slices (demarcated by vertical lines) are shown from EFM flights F2-174–F2-220 covering flight data from full to nearly empty fuel tank. The selected maneuvers are steady heading sideslip (SHSS) and large-amplitude deceleration/acceleration maneuvers, which create significant variations in the body-fixed accelerations and subsequently affect fuel slosh and measured fuel quantity. The total fuel flow is the sum of both measured fuel flow and estimated after-burner consumption. This signal is numerically integrated to the true fuel quantity. The consideration of measurement error leads to the faulty fuel quantity, which is finally compared to the measured fuel quantity. A good fit of measured and faulty fuel quantity is achieved by the application of an appropriate modeling of the fuel slosh impact depending nonlinearly on the three body-fixed measured translational accelerations and on the tank filling ratio.

Center of Gravity

The fuel slosh affects not only the fuel measurement but also the location of the center of gravity and moments of inertia. Here, only the effect on the longitudinal center-of-gravity location is considered. Complementary table data depending on longitudinal and normal accelerations are added to the original weight and balance calculations. The dynamics in the fuel slosh are approximated very

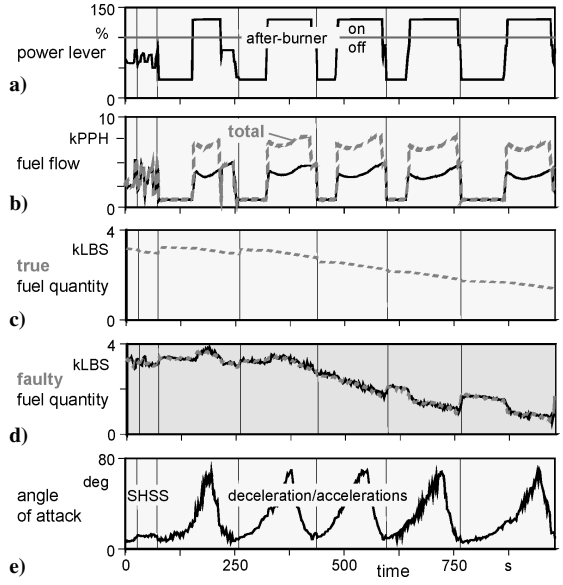

Fig. 7 Fuel quantity estimation: ——, flight data and – – –, model output.

roughly by means of an equivalent time delay and an equivalent rate limitation being likewise applied to the modeling of the fuel measurement error.

Engine Dynamics and Thrust Estimation

The global model uses the original table-based static engine model depending on power lever position, Mach number, and altitude. To match the flight-measured longitudinal acceleration and to enable accurate estimation of drag coefficient, it is necessary to calibrate the original thrust model and to implement generic engine dynamics. The respective evaluation goes in sync with the aerodynamic parameter estimation and is based on deliberately gathered flight data with characteristic power changes covering the entire flight envelope and thrust from idle to maximum after-burner power.

For operations without after-burner, the established dynamic engine model is characterized by first-order dynamics with different time constants and rate limitations for thrust increase and decrease, the rate limitations individually estimated for low- and high-power lever positions. When the output of the first-order engine model exceeds a certain limit, after-burner thrust is added with time lag to simulate the delay in the after-burner ignition. The after-burner switching off is modeled without any delay depending directly on measured power lever with the disengagement level slightly lower than the ignition level.

Measured power lever position is used to drive the dynamic part of the engine model. Its output is used to calculate the thrust from the original static engine tables. Fan and core revolutions per minute, as well as exhaust nozzle area and ambient pressure ratio, serve as additional observation variables for the identification of the engine dynamics. These signals are both in-flight measured and provided by the engine table model. Biases and calibration factors are applied; with respect to thrust, the calibration is estimated individually for after-burner on and off.

Figure 8 shows time histories of a continuous level deceleration/acceleration maneuver (EFM F2-75/7ab) from about 10 up to 70-AOA with piloted, randomly distributed pitch doublets. The power lever is rapidly increased during the test to provide sufficient power for poststall flight, and subsequently, the after-burner is ignited. The effect of the engine dynamics and the after-burner ignition delay can clearly be seen by comparing the measured (solid line) and calculated (dotted line) power lever positions as well as gross thrust calculated without and with engine dynamics. The core-revolutions per minute show a satisfactory fit, although there might be an extra influence of dynamic pressure. To come up with the presented good fit in the longitudinal acceleration, the thrust is identified

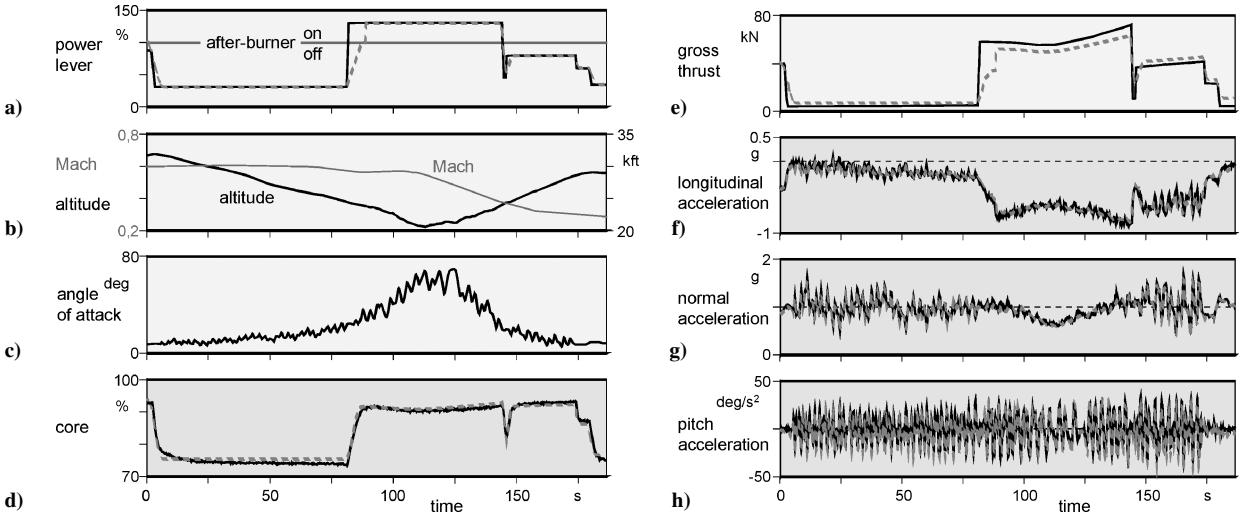

Fig. 8 Engine dynamics and thrust estimation with after-burner: ——, flight data and – – –, model output.

higher than predicted during flight conditions without after-burner and lower than predicted during after-burner operation. Normal and pitch accelerations are presented additionally to demonstrate the overall quality of the identified global model.

Identification of Aerodynamic Parameters

As already mentioned, the global model uses increments to update the original aerodynamic database. These increments depend on angle of attack and Mach number, and they are formulated as aerodynamic derivative tables with nonequidistant breakpoints to be estimated jointly with the other parameters. The use of equidistant breakpoints would not be suitable because, on one hand, only a relative small number of breakpoints can be applied (to keep the total amount of parameters to be estimated within handy limits) and, on the other hand, the X-31A aerodynamic data cover an extended envelope whereas the essential changes in its coefficients are concentrated on some smaller areas. Although the breakpoints were initialized equidistantly, their final estimates are concentrated in the areas with large aerodynamic changes. Furthermore, the estimates of breakpoints are uncorrelated and with small standard deviations, indicating good identifiabilty.

Aerodynamic Model

The global model is separated into a conventional and a high-lift configuration part. The conventional configuration uses, presently, 12 breakpoints for angle of attack (from -5 up to 70 deg) and 6 breakpoints for Mach number (from $\sim$0.2 up to 1.25). At Mach numbers below $\sim$0.2 (corresponding to poststall conditions), the incremental model freezes Mach effect and depends only on AOA. The high-lift configuration uses the AOA breakpoints 2 up to 8 (reaching roughly from -3 up to 26 deg) and Mach breakpoints 1 and 2 (roughly 0.2 and 0.5). The following variables are inputs for the estimation of the incremental derivative tables, each depending on AOA, Mach number, and aircraft configuration. For longitudinal motion the inputs are pitch rate, canard, symmetrical trailing-edge flap, and absolute value of angle of sideslip. For lateral–directional motion, the inputs are angle of sideslip, roll rate, yaw rate, differential trailing-edge flap, and rudder.

Influences of speed brakes and leading-edge flaps are estimated for cruise and high-lift configurations, whereas landing gear is identified for high-lift configuration only. The leading-edge flap deflection is a function of AOA, which is realized in the flight control laws with a dead zone to avoid needless activities at small AOA variations. By the application of the global model with multipoint evaluation, increments for the leading-edge flap effectiveness were estimated uncorrelated to AOA parameters. This is impossible in the case of conventional single-point evaluation.

The number of allocated aerodynamic parameters sums up to $\sim$620 for cruise configuration (including thrust vector effectiveness) and $\sim$420 for high-lift configuration (including landing gear aerodynamics). Some general parameters and spares increase the total to roughly 1300. To cope with engine and landing gear dynamics and their initial values and biases to be estimated for each time slice individually, the maximum number of allocated parameters is expanded to 1700. Of course, a great number of these parameters provided in the global model table formulation are fixed to zero.

After first step-by-step estimations covering limited range of flight variables, the entire flight envelope covering operational AOA and Mach number was analyzed in a final run. Nearly 880 parameters were estimated simultaneously, requiring judicious choice of flight maneuvers analyzed. Because of the earlier described characteristics, the global model approach is applicable to all kinds of maneuvers in the entire flight regime from poststall in very slow subsonic flight up to supersonic flight. Up to 10-h flight-test time, separated in up to 99 time slices, is evaluated in a single identification run with a sampling rate of 12.5 Hz. Thus, all representative flight maneuvers may be gathered for a combined evaluation in cruise, high-lift, and power approach configurations, including their transitions and the acceleration/deceleration segments during takeoff and landing.

Selected Identification Results

Two results are presented and compared to those from single-point evaluation, in some cases already determined during the EFM envelope expansion flight phase. As well-known, a good fit of flight-measured and resimulated time histories is a presumption for reliable system identification results. Such a comparison is shown in Fig. 9, as an example of the global model applicability. The reactions to input sequences as shown in Fig. 5 are shown at about 15- and 65-deg reference AOA (time slices 1 and 2) and additionally two six-degree-of freedom maneuvers, called large-amplitude-maneuvers (time slices 3 and 4) which start at relatively small AOA and are flown far into the PSTs.

The measured accelerations (solid line) show noticeably more noise at high AOA which can be attributed to both the increased activities of the flight control computer for the stabilization of the commanded flight conditions and to the partial separated airflow. Because the resulting airflow turbulence is not included in the model, it is treated as measurement noise. Besides the noise, the flight-measured accelerations are well matched by the simulation results. When simulation of poststall maneuvers is dealt with, it is necessary to include the so-called stall hysteresis[13,14] At fast increasing AOA, the resulting lift is higher than that at decreasing AOA. This is caused by the delayed separation and reattachment of the airflow.

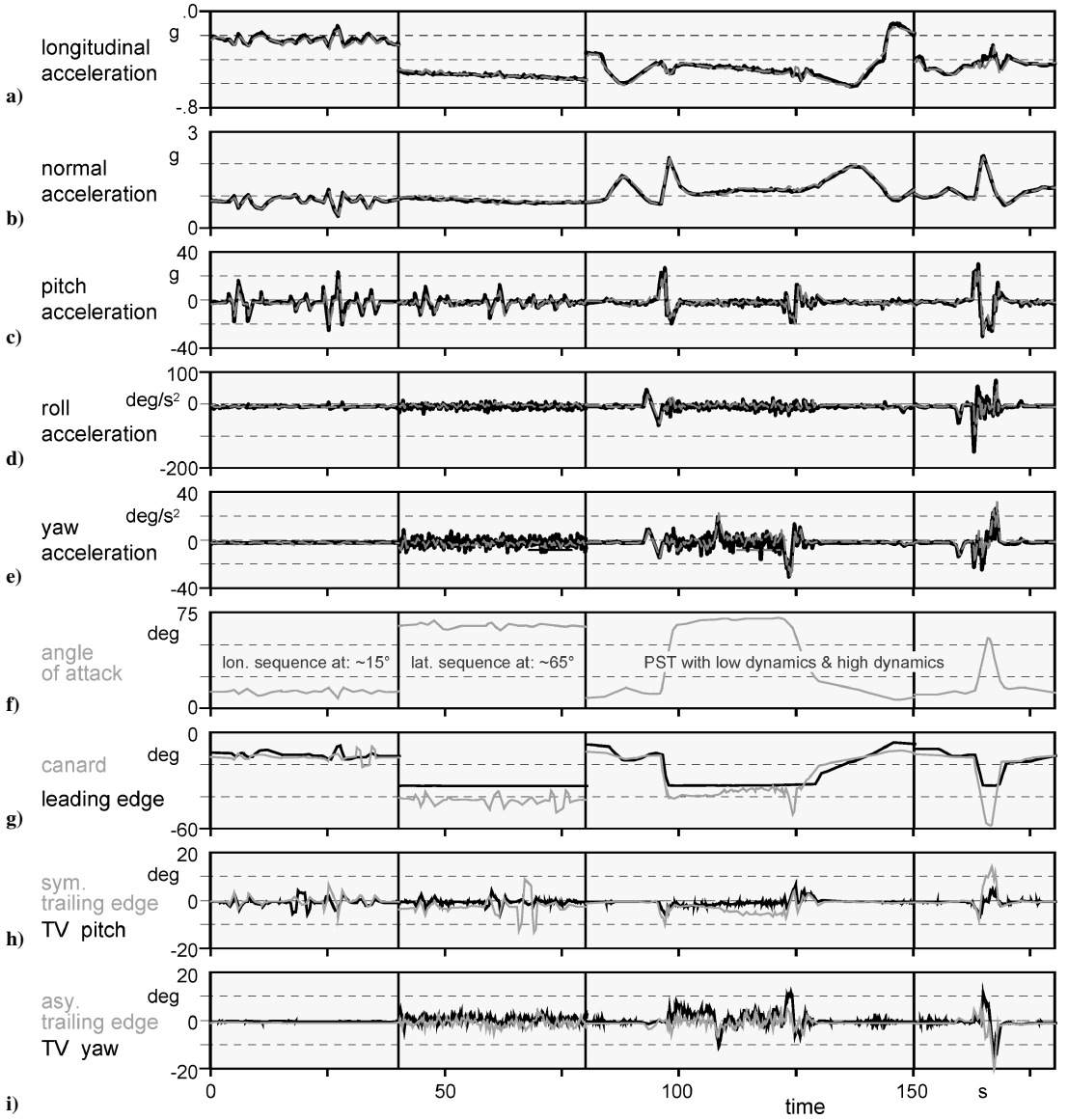

Fig. 9 Flight tests with pilot path and SSE input sequences and post stall maneuvers: ——, flight data and – – –, model output.

During typical envelope expansion flights, the pilot commands the so-called standard maneuvers, for example, doublets in the pitch axes. Such maneuvers and those with single surface excitation can be evaluated by means of linear models at the respective reference point (single-point evaluation). Among others, this leads to the lift coefficient C_{Ltrim} shown and compared to the database predictions in Fig. 10a. Figure 10b shows the result from the evaluation of various standard, SSE, and large-amplitude maneuvers represented by a continuous curve (multipoint evaluation). The error bounds are in both cases too small to be presented here. Not shown is the earlier mentioned hysteresis effect, which has to be superposed to the quasi-static lift coefficient. Differences between the two methods are additionally due to the influence of engine thrust, which can be identified and updated in parallel to the aerodynamics only in the global model evaluation using respective tests with throttle transients. Thus, possible deviations in the thrust model do not affect the identified aerodynamic parameters.

Figure 11 shows the dihedral effect $C_{l\beta}$, comparing the result of both methods to the predictions. At AOA between 25 and 45 deg, the original database has a deep trough that is not validated by the flight-test results. The database was, therefore, updated, at that time based on the EFM single-maneuver evaluation. Subsequently performed global model identification yields nicely matching results, only the range from about 35- up to 45-deg AOA shows a dissimilar trend. This may be due to the model structure that uses a relatively small number of breakpoints and linear interpolation in between. The aerodynamic grid is possibly too rough to cope with the dependency of each of the various derivatives. When the increment $\Delta C_{l\beta}$ is examined, it is obvious that an additional breakpoint between 42 and 55 deg is missing to compensate for the large changes in the original database.

Simulation Update

The results of global model identification, in particular the aerodynamic increments, are written into multidimensional tables and converted into FORTRAN functions at the end of each evaluation run. These functions can be easily implemented into simulations. It is very important to take care when modeling the transients from updated to nonupdated flight regimes being not covered during the flight test. Under well-defined circumstances, the identified increments may be extrapolated, but in most of the cases, it is necessary to fade out the updates within a transition regime. This is valid, especially when the identification is an integrated part of a successive flight regime expansion where each new flight has to be prepared and flown in advance without any failures in a, possibly updated, simulation.[15]

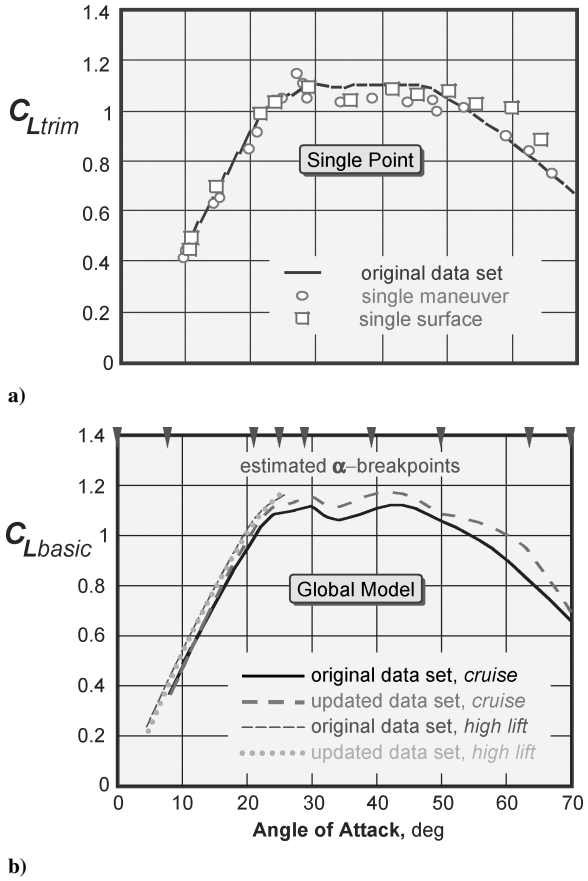

Fig. 10 Lift coefficient, single-point evaluation vs global model evaluation.

Ground Effect Verification and Identification

The latest application of the global model is the verification and identification of ground effect, which changes the aerodynamics significantly during takeoff and landing with the lessening of altitude above ground. At the beginning of the VECTOR project, a ground effect model was developed by CFD calculations at EADS and on the basis of wind-tunnel tests at The Boeing Company. A first flight-test based verification was possible on the basis of multiple manual takeoffs and landings.

In the present case, ground effect must be known with sufficient accuracy for the design of flight control software to enable the automated ESTOL landings. The critical phase of these landings is the reduction of pitch attitude close to the ground, shortly before the main gear touches down. During this derotation maneuver, the lower thrust vector vanes at the aft body of the aircraft represent initially the lowest point that is requested to keep a minimum height of 2 ft (0.6 m) above the runway.

High-Precision Navigation System

After multiple manual landings, it was determined that the integrity beacon landing system (IBLS) of IntegriNautics (Fig. 12) could meet the required high accuracy of approximately 2 cm. Radar altimeter and laser-tracking data were not accurate enough to meet the high accuracy requirements. IBLS is a DGPS navigation system that uses, in addition to the difference signal, the ambiguity of the signal phases in a ground reference station that transmits the calculated correction signal to the X-31A. These data are then used onboard to corroborate the navigation results derived from the three inertial sensor units considering additionally the exactly surveyed profile of the actually selected runway. The low 1-Hz updating rate of the IBLS makes a fusion by means of a Kalman filter necessary. Both systems complement one another perfectly due to their individual system advantages, namely, the dynamic accuracy of the inertial sensor units are combined with the position accuracy of the IBLS.

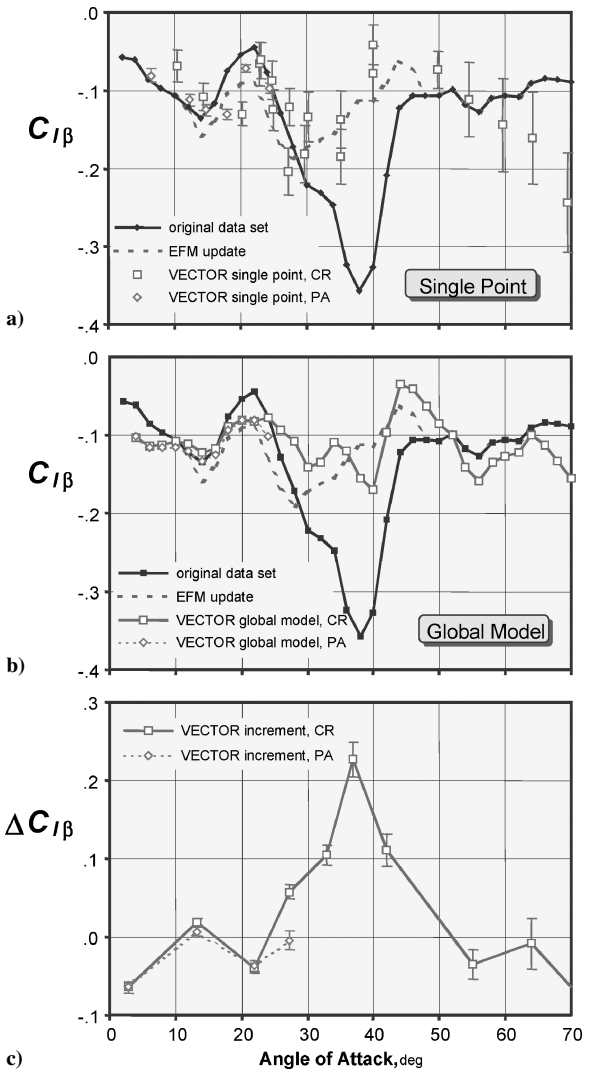

Fig. 11 Dihedral effect, single-point evaluation vs global model evaluation.

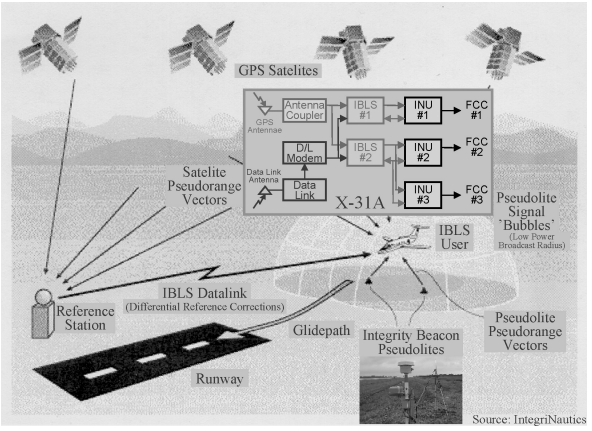

Fig. 12 High-precision landing system IBLS.[6]

Verification of Predictions

The ground effect model was implemented as an additional module of the global model, which, on its side, had to be identified in advance with high accuracy placing special emphasis on the power approach configuration, that is, high-lift configuration with gear down. The combination of the precision navigation system and modern system identification procedure made it possible to verify the predicted ground effect. The obtained results have become part of the initial ESTOL flight clearance procedure.[16]

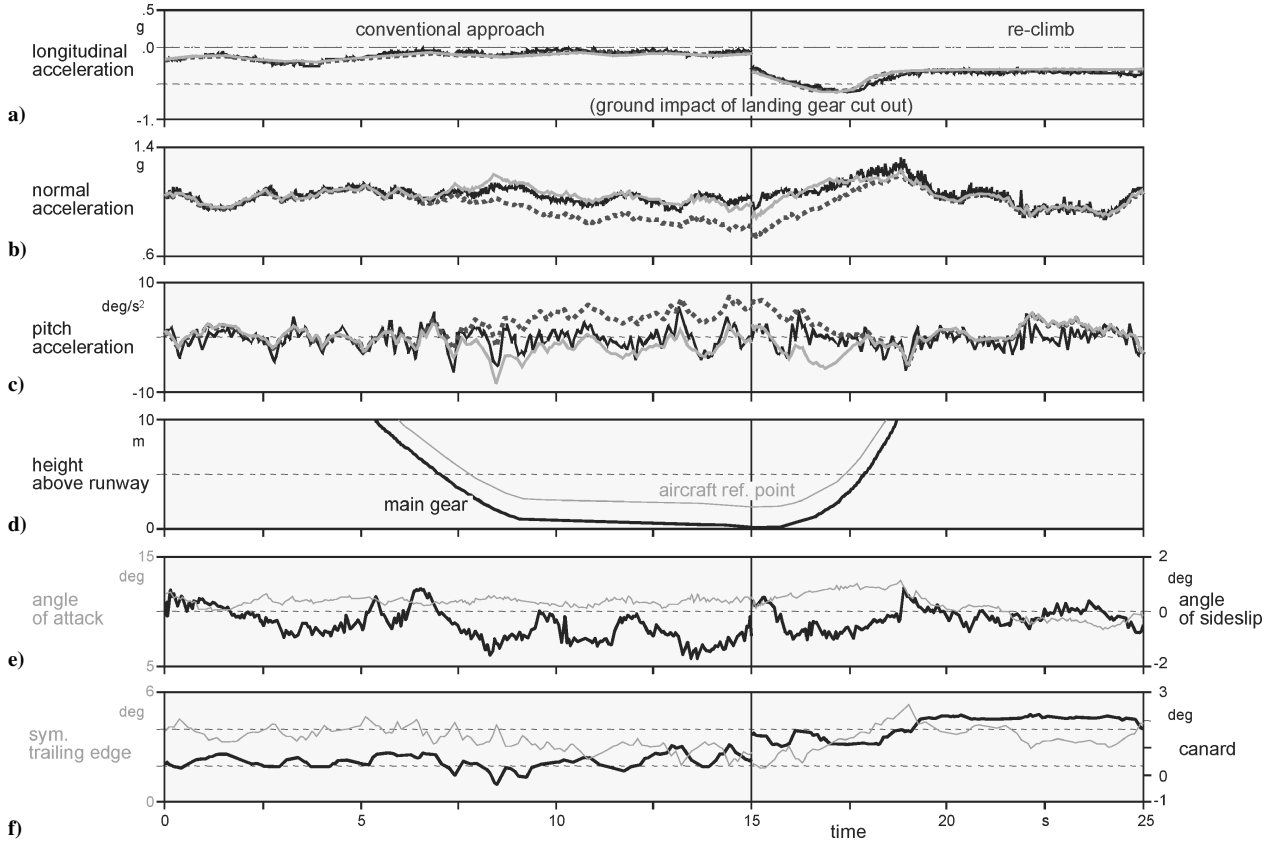

Fig. 13 Resimulation without and with predicted ground effect vs flight test during initial ESTOL to the ground flight clearance process: ——, flight data; · · · ·, model without ground effect; and - - - -, model with predicted ground effect.

Figure 13 shows the measured and resimulated time histories of a conventional touch-and-go maneuver (first touch-and-go of flight F339), but restricted to approach and reclimb. At that time, the landing gear forces could not be simulated with sufficient accuracy to include the few seconds with main gear on ground. Resimulation with predicted ground effect produces a good approximation of the flight measured longitudinal accelerations. To demonstrate the ground effect order of magnitude, the simulated time histories without ground effect are shown additionally. As is well-known, the ground effect helps to reduce the touchdown impact. The aircraft could otherwise pancake due to undersized lift and pitch up, that is, increase AOA and depart. Of course, the X-31A flight control laws would act immediately against this unintended maneuver. To provide a proper picture of the maneuver, Fig. 13 shows additionally the heights of aircraft reference point and main gear above the runway, AOA, and angle of sideslip, as well as the control surface deflections of canard and trailing-edge flaps.

In Fig. 14, flight-test data and resimulated time histories (without and with predicted ground effect) of the longitudinal motion accelerations are presented, in particular, the 18-deg ESTOL touch-and-go of flight F372 and the 24-deg ESTOL landing, the very last X-31 VECTOR landing. The global model can simulate the landing gear forces with sufficient accuracy to make the time segments with ground contact applicable for the identification of the ground effect. The general structure of the generic landing gear module is taken from another system identification application[17] and adapted to the X-31. It was necessary, especially to pinpoint the moment of main gear ground impact, to estimate additional bias parameters for the height above ground, which turned out to be very small, in the range of millimeters to few centimeters. This may be taken as additional evidence of the quality of the onboard determined height above runway. Figure 14 verifies that the predictions are very reliable, even at high AOA during the 18- and 24-deg ESTOL approaches. To illustrate the complexity and dynamic of the automatic ESTOL maneuver, the following additional signals are plotted: height of aircraft reference point above runway and weight on wheels signal, AOA and pitch attitude, as well as the control surface deflections of canard and leading edge flap, trailing-edge flaps and thrust vector, and finally the power lever position and Mach number.

Incremental Ground Effect Identification

Some small improvements were achievable during first identification runs as presented in Fig. 15. The system identification results are derived from the combined evaluation of all analyzable takeoffs and landings, as well as touch-and-go maneuvers of flight F351–F372, either in conventional or in ESTOL control law mode. During the touch-and-go maneuvers, the time history fit is very good, but during takeoff and landings, some model deficiencies are still noted in the normal acceleration. This may be caused by the influence of Mach number, which is not yet considered, or, more probably, due to deficiency in the landing gear model, which is extremely sensitive to height above ground signal. In any case, the high dynamics of the ESTOL maneuvers are correctly resimulated, even the peak of main gear tire acceleration is existent at all touchdowns.

The ground effect, which is modeled with a nonlinear dependence on aircraft height above ground, reduces to zero at a height equivalent to wing span. A hyperbolic formulation was found to be suitable,[18] which is also used in the present case:

$$\sigma = 1 - \tanh(a \cdot h/b) \tag{1}$$

where h is the height above ground and b the wing span. The parameter a characterizes the bending of the curve and is estimated. Figure 16 shows the identified ground effect influence function as a function of non-dimensional height h/b and a flock of curves to illustrate the influence of factor a.

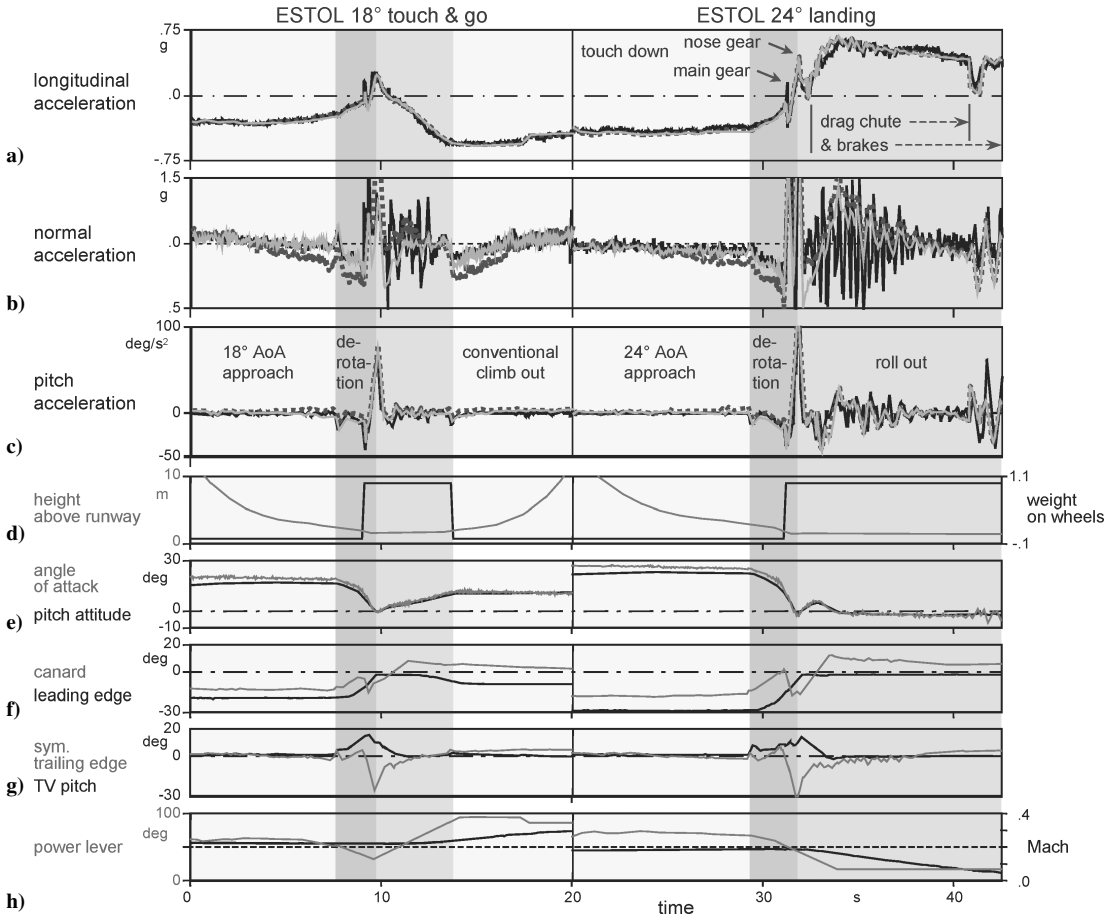

Fig. 14 Resimulation without and with predicted ground effect vs flight test (final ESTOL maneuvers): ——, flight data; · · · ·, model without ground effect and; - - - -, model with predicted ground effect.

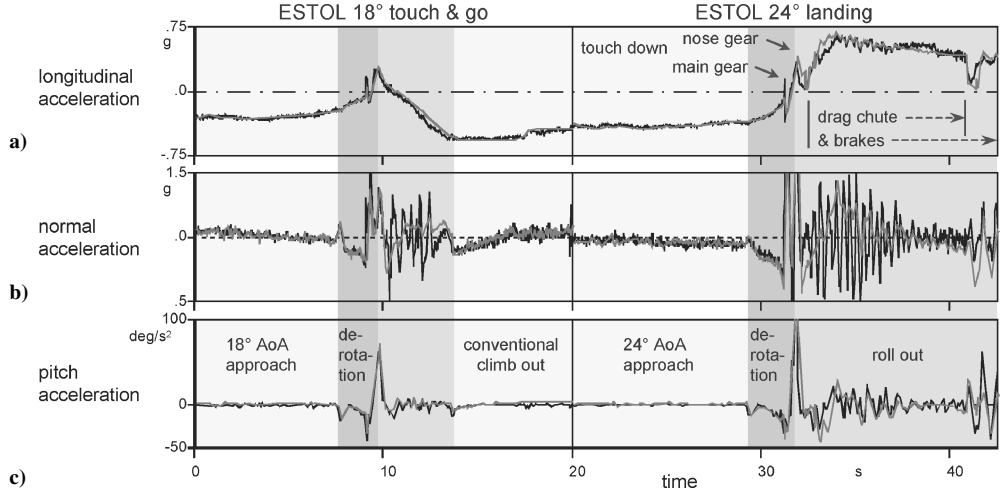

Fig. 15 Resimulated with identified ground effect vs flight test (final ESTOL maneuvers): ——, flight data; and - - - -, model with identified ground effects.

The lift, drag and pitching moment coefficients due to ground effect, [Eqs. (2–4)], are calculated from the original data set and increment tables with the ground effect influence function as input. The incremental formulation uses the same AOA breakpoints as the aircraft high-lift configuration (breakpoints 2 up to 8), but presently no Mach number dependency:

$$C_{Dr,\mathrm{GEe}} = C_{Dr,\mathrm{GEorig}}(\alpha, h/b) + \Delta C_{Dr,\mathrm{GE}}(\alpha, \sigma) \tag{2}$$

$$C_{Li,\mathrm{GEe}} = C_{Li,\mathrm{GEorig}}(\alpha, h/b) + \Delta C_{Li,\mathrm{GE}}(\alpha, \sigma) \tag{3}$$

$$C_{m,\mathrm{GEe}} = C_{m,\mathrm{GEorig}}(\alpha, h/b) + \Delta C_{m,\mathrm{GE}}(\alpha, \sigma) \tag{4}$$

Figures 17a and 17b show ground effect lift coefficient vs dimensionless height above ground, 1) using resimulated time histories and 2) representing the respective ground effect model by a flock of curves with 5-deg AOA variation. Figure 17a shows the predictions and Fig. 17b the estimation results. In each case, the lift coefficient increases more or less hyperbolically with decreasing height (except for $\alpha = 0$). In contrast to the predictions, the identified coefficient shows higher values at very low altitude followed by a sharp drop

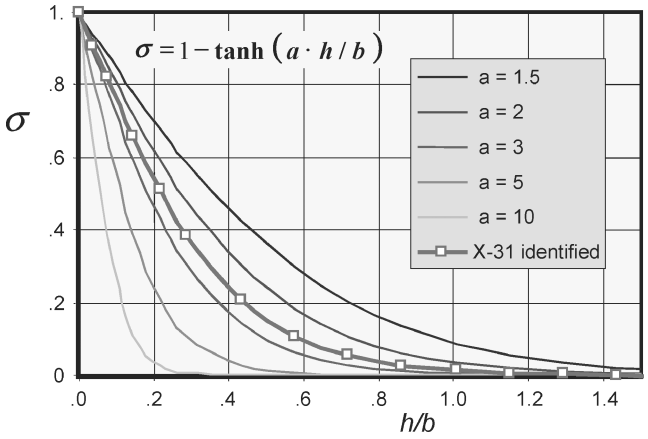

Fig. 16 Ground effect influence function for $\Delta C_{Li,GE}$.

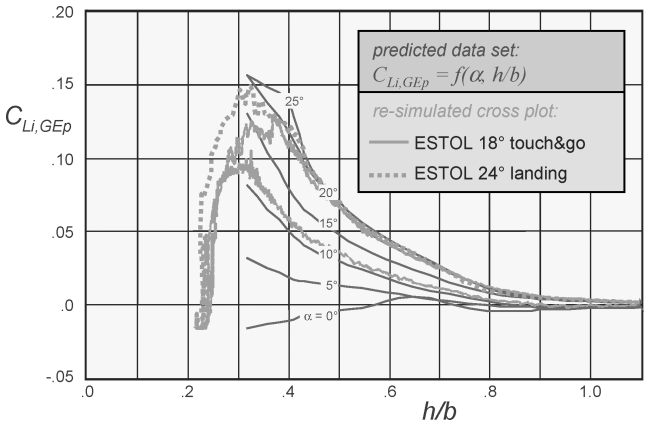

a) Predicted ground effect lift coefficient

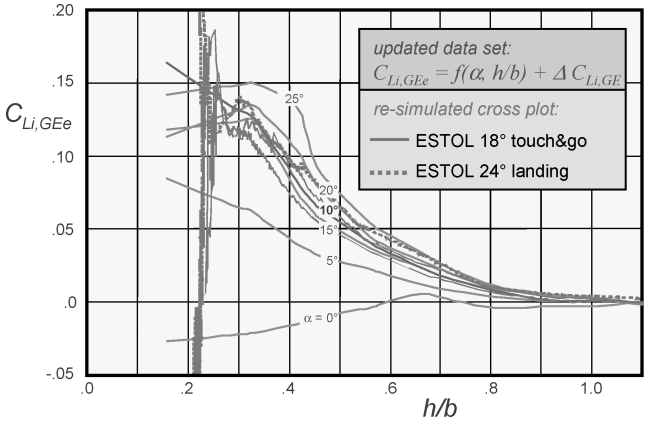

b) Estimated ground effect lift coefficient

Fig. 17 Ground effect lift coefficients vs normalized height above runway.

off after touchdown, representing the fast decrease to negative AOA values. The model predictions are limited due to the wind-tunnel measuring to values above $h/b = 0.32$. The lift coefficient increases with AOA and comes into a saturation above ~20-deg AOA. Below the h/b limit, a linear interpolation routine uses the limit values for AOA dependent ground effect calculation. The identified model does not break off below $h/b = 0.32$ and is characterized by a faster increase at low AOA values with the 10-deg curve being higher than the 15-deg curve and with saturation not as significant as in the predictions. Because flight data with ground effect for low AOA (AOA < 12 deg) are available only when the main landing gear is on ground, at least, there is an interaction with the landing gear forces that calls for further detailed investigations.

Conclusions

A system identification procedure in combination with an innovative global model, developed during the X-31 EFM and X-31 VECTOR programs, leads to dependable identification results that are suitable to resimulate flight data throughout the entire flight regime with high quality. Based on the specially designed flight tests with flight control software generated input signals, aerodynamic increment tables for supplementary update of the original database are identified. Taking advantage of the data provided by a high-precision navigation system, the global model could be extended to interim landing gear and ground effect identification.

The wind-tunnel and CFD-based ground effect model was implemented as a new module into the accurately identified global model, recently as an incremental model supplementing the original data set. Initial identification results from conventional and ESTOL landings show slight improvements compared to the predictions, especially at very low height above ground. Identification of ground effect is an ongoing attempt that is a good example for global model identification, the quality of the results being dependent not only on the aerodynamics but also on other modules, such as fuel slosh, landing gear, and engine submodels.

References

[1]Francis, M. S., "X-31: An International Success Story," *Aerospace America*, Vol. 33, No. 2, pp. 22–27, 32.

[2]Robinson, M. R., and Herbst, W. B., "The X-31A and Advanced Highly Maneuverable Aircraft," *Proceedings of the 17th ICAS Congress*, Vol. 1, International Council of the Aeronautical Sciences, Edinburgh, Uited Kingdom, Sept. 1990, pp. LV–LXIV.

[3]Eubanks, D., Gütter, R., and Lee, B., "X-31 CIC Flight Test Results," *Workshop on Full Envelope Agility*, 4-PWR SM TG, Eglin AFB, March 1995, pp. 31–47.

[4]Friehmelt, H., and Huber, P., "VECTOR—Die X-31A fliegt zu neuen bahnbrechenden Technologiedemonstrationen," *Deutscher Luft- und Raumfahrtkongress 2001*, Paper 2001-090, DGLR, Bonn, Germany, Sept. 2001.

[5]Friehmelt, H., and Jost, M., "Flush Air Data System—An Advanced Air Data System for Aerospace Applications," AIAA Paper 2000-4191-CP, Aug. 2000.

[6]Georg, H.-U., "Aerodynamic Development and Effectiveness Evaluation of the X-31 Thrust Vectoring System," *Fourth High Alpha Conference*, NASA CP-10143, Vol. 2, July 1994.

[7]Beh, H., and Hofinger, G., "Control Law Design of the Experimental Aircraft X-31A," 19th Congress of the International Council of the Aeronautical Sciences, Paper ICAS 94-7.2.1, Sept. 1994.

[8]Weiss, S., Friehmelt, H., Plaetschke, E., and Rohlf, D., "X-31A System Identification Using Single Surface Excitation at High Angles of Attack," AIAA Paper 95-3436, Aug. 1995 .

[9]Friehmelt, H., Grohs, T., and Rohlf, D., "New Challenges and Opportunities for System Identification during VECTOR," RTO-MP-095, Paper 1, Research and Technology Organization, June 2002.

[10]Huber, H., and Galleithner, H., "Control Laws/Flying Qualities and Flight Test Results," *High-Angle-of-Attack Projects and Technology Conference*, NASA-CP-3137, Vol. 1, April 1992, pp. 171–188.

[11]Rohlf, D., "Direct Update of a Global Simulation Model with Increments via System Identification," RTO-MP-11, Paper 28, March 1999.

[12]Weiss, S., Friehmelt, H., Plaetschke, E., and Rohlf, D., "X-31A System Identification Using Single Surface Excitation at High Angles of Attack," *Journal of Aircraft*, Vol. 33, No. 3, 1996, pp. 485–490.

[13]Hamel, P. G., "Advances in Aerodynamic Modeling for Flight Simulation and Control Design," GAMM-Mitteilungen, Vol. 1/2, Wiley–VCH, Berlin 2000, pp. 7–50.

[14]Jategaonkar, R., Fischenberg, D., and von Gruenhagen, W., "Aerodynamic Modeling and System Identification from Flight Data—Recent Applications at DLR," *Journal of Aircraft*, Vol. 41, No. 4, 2004, pp. 681–691.

[15]Friehmelt, H., and Rohlf, D., "Fast Model Updates and Simulation for Efficient Flight Control Software Design," *13th International Federation of Automatic Control Symposium on System Identification*, Paper 407, Aug. 2003.

[16]Heinzinger, O., Fischer, B., and Grohs, T., "X-31 VECTOR—Die Entwicklungsstufen der ESTOL-Regelung bis zur Bodenlandung," DGLR-Jahrestagung, Paper 2003-055, Nov. 2003. (in German).

[17]Fischenberg, D., and Moennich, W., "C-160 Ground Handling Model Update Using Taxi Test Data," CP-577, AGARD, April 1996, pp. 12-1–12-8.

[18]Fischenberg, D., "Ground Effect Modeling Using a Hybrid Approach of Inverse Simulation and System Identification," AIAA Paper 99-4324-CP, Aug. 1999.